Journal of Magnetic Resonance **154,** 60–72 (2002)
doi:10.1006/jmre.2001.2458, available online at http://www.idealibrary.com on IDEAL®

NMR of Multipolar Spin States Excited in Strongly Inhomogeneous Magnetic Fields

A. Wiesmath, C. Filip, D. E. Demco, and B. Blümich[1]

Institut für Technische Chemie und Makromolekulare Chemie, Rheinisch-Westfälische Technische Hochschule, Worringerweg 1, D-52056 Aachen, Germany

Received June 19, 2001; revised October 18, 2001

The possibility of exciting and filtering various multipolar spin states in proton NMR like dipolar encoded longitudinal magnetization (LM), double-quantum (DQ) coherences, and dipolar order (DO) in strongly inhomogeneous static and radio-frequency magnetic fields is investigated. For this purpose pulse sequences which label and manipulate the multipolar spin states in a specific way were implemented on the NMR-MOUSE (mobile universal surface explorer). The performance of the pulse sequences was also tested in homogeneous fields on a solid-state high-field NMR spectrometer. The theoretical justification of these procedures was shown for a rigid two-spin 1/2 system coupled by dipolar interactions. Dipolar encoded longitudinal magnetization decay curves, double-quantum and dipolar-order buildup curves, as well as double-quantum decay curves were recorded with the NMR-MOUSE for natural rubber samples with different crosslink density. The possibility of using these multipolar spin states for investigations of strained elastomers by NMR-MOUSE is also shown. These curves give access to quantitative values of the ratio of the total residual dipolar couplings of the protons in the series of samples which are in good agreement with those measured in homogeneous fields.

Key Words: **double-quantum NMR coherences; dipolar order; dipolar encoded longitudinal magnetization; multipolar spin states; NMR-MOUSE; cross-linked natural rubber; strain.**

1. INTRODUCTION

Over the past few years, several new NMR applications have been developed for use in strongly inhomogeneous static and radio-frequency magnetic fields. Applications include materials testing (*1–4*), well logging for oilfield applications (*5*), and stray field NMR (*6*). It has been shown that for protons various NMR parameters like T_1 (*3*), T_2 (*2, 7, 8*), $T_{1\rho}$ (*2, 9*), and self-diffusion coefficients (*10*) can be measured under these conditions. Moreover, van Vleck moments of ^{1}H residual dipolar couplings can be measured from the accordion magic sandwich (*11*). The possibility of exciting ^{1}H double-quantum (DQ) coherences in strongly inhomogeneous fields was also shown (*12*), extending the application of this technique to elastomers (*13, 14*) and ordered tissues (*15*) in homogeneous fields.

Recently, a mobile NMR surface scanner (NMR-MOUSE is a trademark of RWTH, Peter Blümler and Bernhard Blümich) was developed for the nondestructive investigation of arbitrarily large objects (*1–4*). The NMR-MOUSE is a palm-size NMR device and is characterized by strong inhomogeneities in the static and radio frequency magnetic fields (*7*). Due to these inhomogeneities the task to implement specific NMR techniques is not trivial.

The aim of this paper is to investigate the possibility of exciting multipolar spin states in strongly inhomogeneous fields using the NMR-MOUSE. These multipolar spin states or spin modes correspond mainly to longitudinal magnetization (LM) or polarization, multiple-quantum (MQ) NMR coherences, and spin order (*16, 17*, and references therein). The dipolar and quadrupolar states are conveniently described, especially for the last case, by the irreducible tensor operators $\mathbf{T}_{l,p}$ of rank l and order p (see, for instance, Ref. (*16*)). For a dipolar coupled spin-1/2 pair or a quadrupolar nuclei with spin $I = 1$, the irreducible tensor operators $\mathbf{T}_{1,0}$, $\mathbf{T}_{2,\pm2}$, and $\mathbf{T}_{2,0}$ correspond to longitudinal magnetization, double-quantum (DQ) coherences, and dipolar order (DO), respectively. Recently, it was shown that for dipolar coupled spins the multipolar LM state is encoded by the dipolar interactions (*13*). A spin multipolar state which is not present for quadrupolar nuclei is the zero-quantum coherence (ZQ). Nevertheless, for isolated spin-1/2 pairs with different chemical shifts the selective excitation of one resonance can convert DQ coherences into ZQ coherences (*18*). For obvious reasons, this procedure cannot be applied in strongly inhomogeneous magnetic fields. In a dipolar multi-spin network the pulse sequences used for excitation of DQ coherences will also excite ZQ coherences and dipolar encoded LM. The response of the LM, ZQ, and DO to the phase cycling of rf pulses is the same making the separation of these states difficult. Nevertheless, in general, the life times of DQ and ZQ coherences are very different from that of dipolar encoded LM and DO, which is related to the spin–lattice relaxation times T_1 and T_{1D}, respectively. These features can be used together with other procedures for filtering these multipolar spin states (see below).

We must mention that in strongly inhomogeneous fields the existence of a broad flip-angle distribution of rf pulses precludes the implementation of some filtration experiments.

[1] To whom correspondence should be addressed.

1090-7807/02 $35.00

For instance, orientationally ordered ^{23}Na ions can be distinguished from the bulk of sodium ions by means of a simple flip-angle effect in a DQ-filtered experiment (*19, 20*). This effect will be present in just a few voxels of the sample for the NMR-MOUSE. Fortunately, there are other experiments which work in the presence of strong field inhomogeneities. As an example, the Jeener–Broekaert experiment (*21*), producing multipolar states of dipolar or quadrupolar order, does not relay upon the flip-angle effect to suppress the unwanted signal components (*22–24*). The required discrimination arises as a result of the nominal 90° pulse and the first nominal 45° pulse having orthogonal phases. This phase condition can be fulfilled for all the voxels in the sample in the presence of strongly inhomogeneous fields. Moreover, rf pulse phases well defined over the sensitive volume enable one to use well established phase cycling procedures (*25, 26*) for filtering DQ coherences and dipolar encoded longitudinal magnetization.

The paper is organized as follows: In Section 2 we present the spin system response for a spin-1/2 pair to the pulse sequences used for the excitation of dipolar encoded LM, DQ coherences, and DO. To mimic partially, the inhomogeneities of magnetic fields an arbitrary flip angle of rf pulses were considered. Under these conditions the simultaneous excitation of various multipolar spin states was shown to be effective. The measurements were performed on the important class of elastomer materials. The experiments and samples are described in detail in Section 3. The effects of crosslinking and strain on the multipolar spin states were investigated for natural rubber. These results are presented in Section 4 and compared with the measurements of multipolar states generated in homogeneous magnetic fields.

2. THEORY

2.1. Excitation of Dipolar Encoded LM and DQ Coherences

The most simple method to excite and detect MQ coherences exploits time reversal procedure (cf. Fig. 1a) like the nonselective three-pulse sequence (*25, 26*) or its variant presented in Fig. 1b. Here the duration of excitation and reconversion periods are equal and the efficiency in pumping MQ coherences is increasing in the initial excitation/reconversion time regime. A build-up curve is recorded in this case for which a maximum is present as a result of the competitive effects of pumping MQ coherences and transverse relaxation of single-quantum coherences (*13*).

We shall consider in the following the spin system response to the pulse sequence of Fig. 1b used for the excitation of MQ coherences. The case of a rigid, magnetically equivalent, isolated two spin-1/2 system will be treated excited by radio-frequency pulses having well-defined arbitrary flip angles. This will allow us the possibility to investigate the multipolar spin states which can be excited by NMR-MOUSE, i.e., in strongly inhomogeneous magnetic fields where a distribution of pulse flip angles exist. Nevertheless, the radio-frequency pulse phases are not distributed over the sample volume. They are the same for each voxel.

The spin system response for an isolated, magnetically equivalent two spin-1/2 system can be described by an equivalent quadrupolar nucleus with spin $I = 1$ (see for instance, Ref. (*27*)). Under the action of the pulse sequence presented in Fig. 1b the reduced density operator σ can be conveniently described at various moments of time in terms of the irreducible tensor operators $T_{l,p}$. The effect of partial refocusing by 2θ rf pulses (cf. Fig. 1b) will be neglected in the following, being not essential for the

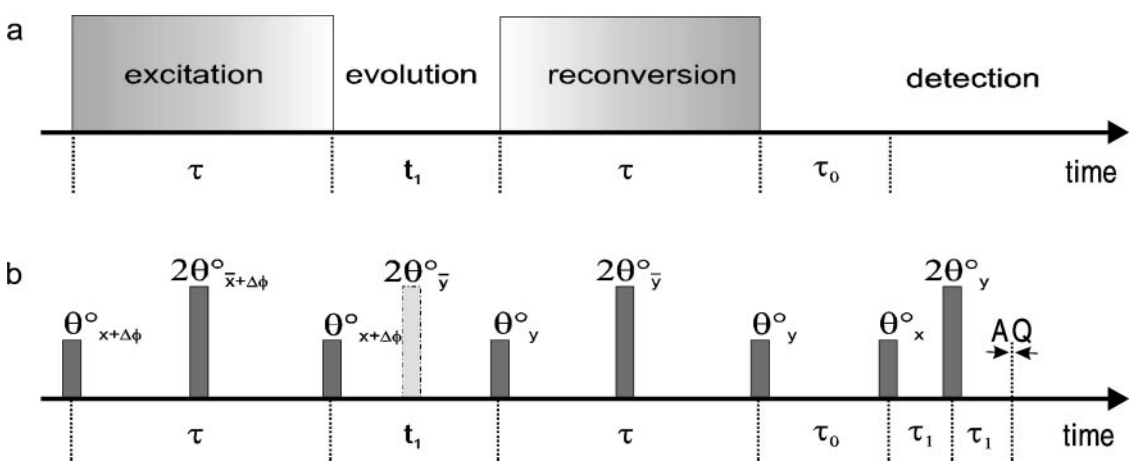

FIG. 1. (a) General scheme for filtering NMR signals according to dipolar encoded LM and MQ coherences. This scheme is similar to a two-dimensional MQ experiment but it is used with fixed evolution time t_1 and variable, but equal, excitation/reconversion times τ. (b) A five-pulse sequence with an arbitrary pulse flip angle θ, supplemented by 2θ pulses for partial refocusing to measure dipolar encoded LM and DQ filtered signals with variable excitation/reconversion times. The evolution time t_1 is kept short and constant and a 2θ pulse (represented by a gray area) is applied at the middle of this interval for partially refocusing the DQ coherences evolution under inhomogeneous Hamiltonians. This pulse is applied in alternative scans for dipolar encoded LM experiments. The z filter is represented by the last θ pulse of the reconversion period and a free evolution period of duration τ_0. The detection in strongly inhomogenous magnetic fields is achieved by a Hahn echo. The phase cycling schemes used in the experiments are listed in Tables 1 and 2.

filtration of DQ coherences. Nevertheless, these pulses refocus the fast coherence decay of inhomogeneous nature, being essential for the success of the experiment. The experiment starts with the spin system exhibiting z polarization, i.e., $\sigma(0^-) \propto T_{1,0}$. After the action of the first hard θ pulse

$$\sigma(0^+) \propto T_{1,0}\cos\theta + iT_{1,1}(s)\sin\theta, \qquad [1]$$

where $T_{1,1}(s)$ is the symmetric irreducible tensor operator of $T_{1,\pm1}$ defined as $iT_{1,1}(s) = (1/\sqrt{2})[T_{1,1} + T_{1,-1}]$, (*17*).

Under the effect of truncated residual dipolar Hamiltonian $\bar{H}_{\rm d}^{(0)} = \bar{\omega}_{\rm d}T_{2,0}$, where $\bar{\omega}_{\rm d}$ is the preaveraged intra- and intergroup dipolar coupling constant in elastomers (*28* and references therein) the density operator at the end of the first free evolution period of duration τ (cf. Fig. 1b) is given by

$$\sigma(\tau^-) \propto T_{1,0}\cos\theta + iT_{1,1}(s)\cos\left(\sqrt{\frac{3}{2}}\bar{\omega}_{\rm D}\tau\right)\sin\theta + \sqrt{2}T_{2,1}(a)\sin\left(\sqrt{\frac{3}{2}}\bar{\omega}_{\rm D}\tau\right)\cos\theta, \qquad [2]$$

where the antisymmetric combination of the irreducible tensor operators $T_{2,\pm1}$ is given by $T_{2,1}(a) = \frac{1}{\sqrt{2}}[T_{2,1} - T_{2,-1}]$, (*17*). In Eq. [2] all the relaxation processes have been neglected.

After the action of the second rf θ pulse (cf. Fig. 1b), the density operator is given by

$$\sigma(\tau^+) \propto T_{1,0}\cos^2\theta - T_{1,0}\sin^2\theta\cos\left(\sqrt{\frac{3}{2}}\bar{\omega}_{\rm D}\tau\right) + \frac{i}{2}T_{1,1}(s)\sin 2\theta + \frac{i}{2}T_{1,1}(s)\sin 2\theta\cos\left(\sqrt{\frac{3}{2}}\bar{\omega}_{\rm D}\tau\right) + \frac{\sqrt{2}}{2}T_{2,1}(a)\sin 2\theta\sin\left(\sqrt{\frac{3}{2}}\bar{\omega}_{\rm D}\tau\right) + i\sqrt{2}T_{2,2}(a)\sin^2\theta\sin\left(\sqrt{\frac{3}{2}}\bar{\omega}_{\rm D}\tau\right). \qquad [3]$$

Therefore, at the end of the excitation period dipolar encoded and nonencoded longitudinal magnetization ($T_{1,0}$), dipolar encoded and nonencoded single-quantum coherences ($T_{1,1}(s)$), dipolar encoded antiphase single-quantum coherences ($T_{2,1}(a)$), and dipolar encoded double-quantum coherences ($T_{2,2}(a)$) have been excited. It is also evident that no dipolar order or zero-quantum coherences are present. This fact is also valid for DO in the case of dipolar coupled multi-spin systems or quadrupolar nuclei with $I > 1$. Nevertheless, based on the selection rules valid for MQ NMR spectroscopy (*25, 26, 29, 30*) ZQ coherences are excited by the nonselective three pulse sequence for a dipolar network with the number of spins $N > 2$.

LM and DQ multipolar spin states can be filtered from the other coherences and from each other by specific phase cycling schemes (see below). From Eq. [3] the density operators describing LM and DQ multipolar spin states are given at the end of excitation period by

$$\sigma_{\rm LM}(\tau^+) \propto T_{1,0}\cos^2\theta - T_{1,0}\sin^2\theta\cos\left(\sqrt{\frac{3}{2}}\bar{\omega}_{\rm D}\tau\right) \qquad [4]$$

and

$$\sigma_{\rm DQ}(\tau^+) \propto i\sqrt{2}T_{2,2}(a)\sin^2\theta\sin\left(\sqrt{\frac{3}{2}}\bar{\omega}_{\rm D}\tau\right), \qquad [5]$$

respectively.

At the end of the reconversion period and the z-filter of duration τ_0 (cf. Fig. 1) the LM and DQ encoded z polarizations can be evaluated using the procedure discussed above. Finally the LM and DQ filtered normalized signals originating from a θ voxel are given by

$$\frac{S_{\rm LM}^{\theta}(\tau_0+2\tau)}{S_0} \propto \cos^4\theta + \sin^4\theta\left\langle\cos^2\left(\sqrt{\frac{3}{2}}\bar{\omega}_{\rm D}\tau\right)\right\rangle, \qquad [6]$$

and

$$\frac{S_{\rm DQ}^{\theta}(\tau_0+2\tau)}{S_0} \propto \sin^4\theta\left\langle\sin^2\left(\sqrt{\frac{3}{2}}\bar{\omega}_{\rm D}\tau\right)\right\rangle, \qquad [7]$$

respectively. In Eqs. [6] and [7] the evolution of LM and DQ multipolar spin states during the t_1 period was neglected and S_0 is the SQ signal detected by a Hahn echo with a short echo time. Furthermore, the relaxation of coherences characterized by an effective relaxation time $T_{2,\rm eff}$ during excitation and reconversion periods can be neglected for $\tau \ll T_{2,\rm eff}$. The symbol $\langle(\ldots)\rangle$ represents the averages taken over the orientation of spin-pair internuclear vector and the statistics of the end-to-end vectors (see, for instance, Ref. (*13*)). In the case of the NMR-MOUSE, Eqs. [6] and [7] describe the signals originating from a particular sample voxel characterized by an rf pulse having a θ flip angle. The total, filtered signals can be evaluated as in Ref. (*7*), and the relevant part is given by an integral which include *inter alia* the space distribution of the flip angles. This integral can be performed numerically from given distribution of the static and radio-frequency fields (*7*) and is expressed by the symbol $\langle(\ldots)\rangle_\theta$. From Eqs. [6] and [7] one finally gets

$$\frac{S_{\rm LM}(\tau_0+2\tau)}{S_0} \propto \langle\cos^4\theta\rangle_\theta + \langle\sin^4\theta\rangle_\theta\left\langle\cos^2\left(\sqrt{\frac{3}{2}}\bar{\omega}_{\rm D}\tau\right)\right\rangle \qquad [8]$$

and

$$\frac{S_{\mathrm{DQ}}(\tau_0+2\tau)}{S_0} \propto \langle \sin^4\theta\rangle_\theta \left\langle \sin^2\left(\sqrt{\frac{3}{2}}\bar{\omega}_{\mathrm{D}}\tau\right)\right\rangle. \qquad [9]$$

If the excitation/reconversion intervals τ fulfill the conditions $\bar{\omega}_{\mathrm{D}}\tau \ll 1$, and $\tau \ll T_{2,\mathrm{eff}}$ the above equations can be approximated by

$$\frac{S_{\mathrm{LM}}(\tau_0+2\tau)}{S_0} \propto \langle \cos^4\theta\rangle_\theta + \langle \sin^4\theta\rangle_\theta \left(1-\frac{3}{2}\langle(\bar{\omega}_{\mathrm{D}})^2\rangle\tau^2\right) \qquad [10]$$

and

$$\frac{S_{\mathrm{DQ}}(\tau_0+2\tau)}{S_0} \propto \langle \sin^4\theta\rangle_\theta \frac{3}{2}\langle(\bar{\omega}_{\mathrm{D}})^2\rangle\tau^2. \qquad [11]$$

The derivative of the LM decay curve and DQ buildup curve taken over the variable τ^2 in this initial time regime yields a quantity related to the square of the total (inter- and intrafunctional groups) residual dipolar couplings of the elastomer segments.

For a multi-spin dipolar topology the effect of pumping DQ high-order spin correlations and high-order MQ coherences leads to a more complex treatment as that described above. Nevertheless, the above equations are expected to be valid in the regime of short excitation/reconversion times (*13*).

2.2. Dipolar Order Build-up Curve

The excitation of the DO multipolar spin state can be achieved by the Jeener–Broekaert pulse sequence (*21*). This pulse sequence was adapted to the NMR-MOUSE sensor and it is shown in Fig. 2. The scheme is similar to that used for excitation of LM and MQ multipolar spin states and possesses preparation (sample polarization), excitation, evolution, and reconversion periods (cf. Fig. 2a). The spin system response to the action of the pulse sequence of Fig. 2b can be evaluated under the same conditions as discussed in the previous section. Using the relationship given in Ref. (*16*) for the evolution of irreducible tensor operators under the dipolar interaction and rf pulses we can write for the density operator at the end of the excitation period

$$\begin{aligned}\sigma(\tau^+) \propto\ & T_{1,0}\cos(\theta/2)\cos\theta + T_{1,1}(a)\sin(\theta/2)\cos\theta \\ & + iT_{1,1}(s)\sin\theta\cos\left(\sqrt{\frac{3}{2}}\bar{\omega}_{\mathrm{D}}\tau\right) \\ & - i\frac{\sqrt{2}}{2}\left[\sqrt{3}T_{2,0}\sin^2\theta - T_{2,1}(a)\sin(2\theta) - T_{2,2}(s)\sin^2\theta\right] \\ & \times \sin\left(\sqrt{\frac{3}{2}}\bar{\omega}_{\mathrm{D}}\tau\right). \end{aligned} \qquad [12]$$

It is evident that at the end of the excitation period, multipolar spin states of LM, SQ, DQ, and dipolar order are produced. The last spin state is described by the irreducible spin operator $T_{2,0}$. If the evolution period t_1 is longer than the transverse relaxation times of SQ and DQ coherences only the LM (or Zeeman order), which is now not encoded by the dipolar interaction, and the DO will survive. The 2θ pulse applied in the middle of the evolution period (cf. Fig. 2b) will change the sign of the LM allowing a partial filtering of this spin state (see below). The signal detected in phase with the last $\theta/2$ pulse is encoded only by the DO as in a

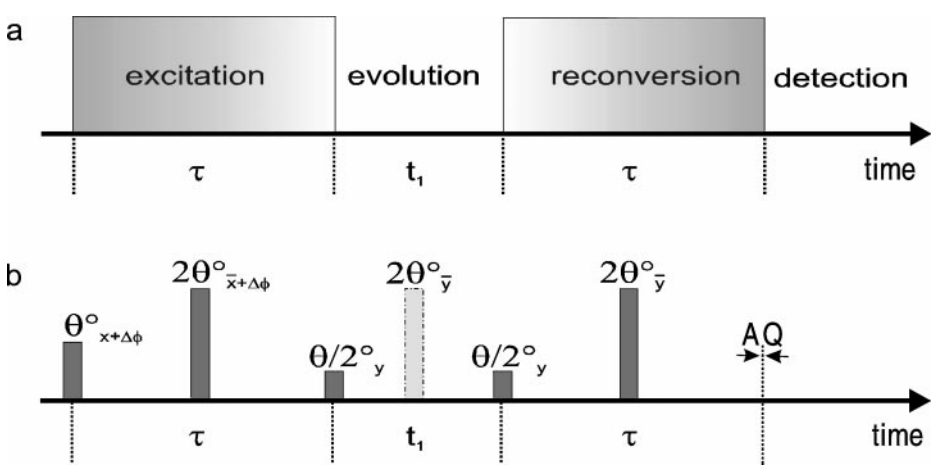

FIG. 2. (a) General scheme for recording dipolar order build-up curves based on the Jeener–Broekaert experiment (*21*). The evolution time t_1 is kept fixed and only the excitation/reconversion time τ is varied. (b) Jeener–Broekaert three-pulse sequence with arbitrary flip angles θ and $\theta/2$, supplemented by 2θ partially refocusing pulses. The evolution time t_1 is kept constant and long enough so that DQ and ZQ coherences will irreversibly be dephased. A 2θ pulse (represented by a gray area) is applied in alternate scans at the middle of the t_1 interval for partially filtering of the LM spin state. The amplitude of the dipolar echo is detected. The phase cycle employed is listed in Table 3.

Jeener–Broekaert experiment (*21*) performed with 45° pulses. It can be easily shown from the above results that the normalized spin state of DO detected at the maximum of the transferred dipolar echo is given by

$$\frac{S_{\mathrm{DO},y}(2\tau)}{S_0} \propto \frac{3}{4}\langle \sin^3\theta\rangle_\theta \left\langle \sin^2\left(\sqrt{\frac{3}{2}}\bar{\omega}_{\mathrm{D}}\tau\right)\right\rangle. \qquad [13]$$

The above equation is valid for small t_1 values when the spin–lattice relaxation of the dipolar order can be neglected. For the case of spin-1/2 pairs the dipolar encoding of DQ and DO is the same (cf. Eqs. [9] and [13]), but the flip angle encoding is different. Therefore, as for the DQ case, a DO build-up curve can be recorded when the excitation/reconversion time τ is incremented. In the initial excitation regime from Eq. [13] the NMR signal filtered for DO is given by

$$\frac{S_{\mathrm{DO},y}(2\tau)}{S_0} \propto \frac{9}{8}\langle \sin^3\theta\rangle_\theta \langle(\bar{\omega}_{\mathrm{D}})^2\rangle \tau^2, \qquad [14]$$

when the transverse relaxation of coherences during excitation/reconversion period is neglected.

We can mention here that the DO build-up curves which can be recorded by the changes in the excitation/reconversion times τ (cf. Fig. 2a) are not limited to spin-1/2 pairs or quadrupolar nuclei with spin $I = 1$. This effect can be also detected for a dipolar-coupled multi-spin network as is evident from the results of Jeener and Broekaert (*21*). The inverse spin temperature associated with the dipolar reservoir reaches a maximum when

$$\left|\frac{d}{d\tau}G(\tau)\right|$$

is maximum, where the function $G(\tau)$ describes the free induction decay.

3. EXPERIMENTAL

3.1. Samples

A series of differently cross-linked elastomer samples based on commercially available natural rubber (NR) SMR10 (Malaysia) was investigated. The additives were 3 phr (*p*arts-per-*h*undred-*r*ubber) ZnO and 2 phr stearic acid. The sulfur and accelerator contents are 1-1 phr for the sample NR1 and 5-5 phr for NR5. The accelerator is of the standard sulfenamide type (TBBS, benzothiazyl-2-*tert*-butyl-sulfenamide). After mixing the compounds in a laboratory mixer at 50°C, the samples were vulcanized at 160°C in a Monsanto MDR-2000-E vulcameter. The degree of cross-linking was measured by the low frequency shear modulus at a temperature of 160°C in the vulcameter directly after the vulcanization. The measurements were performed with an oscillation amplitude of ±0.5° and a frequency of 1.67 Hz.

For the experiments performed under mechanical stress, a simple home-built stretching device was used. The natural rubber bands had the dimensions of 180 × 35 × 4 mm in the unstrained state. The NMR-MOUSE was positioned below the rubber band in contact with the surface of the rubber band. The width of the band was larger than the diameter of the radio-frequency coil of 13 mm.

3.2. NMR Experiments

The ^{1}H NMR experiments in inhomogeneous fields were performed with a home made NMR-MOUSE sensor equipped with a Bruker Minispec spectrometer operating at a carrier frequency of 20.1 MHz and a coil geometry with a sensitive volume of about 9 × 4 mm in plane and 0.5 mm in depth. Further details are published in Ref. (*1*). The length of a pulse employed in all the measurements had a value of 2.5 μs, the z-filter time was $\tau_0 =$ 500 μs, and the Hahn echo time was $\tau_1 = 100$ μs (cf. Figs. 1b and 2b). The evolution time was $t_1 = 60$ μs, $t_1 = 100$ μs, and $t_1 = 60$ μs for DQ, DO, and LM experiments, respectively. The DQ decay curves were recorded using the MERE pulse sequence (*12*) with a fixed value of $\tau = 1$ ms, and $\tau = 0.8$ ms corresponding to the maximum of the DQ buildup curves for the sample NR1 for two extension ratios $\lambda = 1.00$ and 2.25, respectively. The intensity of the DQ filtered signals for two different excitation/reconversion times $\tau = 0.5$ and 1.6 ms taken around the value of τ corresponding to the maxim of the build-up curve was measured for the NR1 band with $\lambda = 2.5$ versus the angle Θ between the direction perpendicular on the magnet poles and the direction of the stretching force. This measurements can be easily performed with the NMR-MOUSE sensor.

The NMR experiments in homogeneous fields were performed at a ^{1}H frequency of 500.045 MHz on a Bruker DSX-500 solid-state spectrometer. The 90° pulse length was 2 μs. To partially mimic the effect of rf pulse inhomogeneities the LM and DO filtered signals were recorded with an rf pulse flip angle of about $\theta = 60°$. The same pulse delays were used as for the measurements performed with the NMR-MOUSE. The acquisition was performed without employing a Hahn echo. Partial refocusing was achieved by applying 2θ pulses in the middle of the excitation, evolution, and reconversion periods (cf. Figs. 1b and 2b and the discussion below).

Phase cycling schemes for detecting dipolar encoding LM (*13, 14*), DQ coherences (*25, 26*), and DO (*22, 24*) filtered signals were applied in all experiments. The basic phase cycles without CYCLOPS are presented in Tables 1 to 3. In the DQ experiments, ZQ coherences (and also LM) are filtered out by the classical phase cycle (*25, 26*). For the experiment concerning the multipolar LM state, the difference of the filtered signals recorded with and without the 2θ refocusing pulse was taken. The refocusing pulse will not change the sign of the ZQ and DQ coherences. Because of ZQ coherence, dipolar encoded

TABLE 1
Basic Phase Cycling Scheme Used for Recording Dipolar Encoded LM

	Radio-frequency pulse and receiver phases							
P1	x	x	y	y	−x	−x	−y	−y
P2	−x	−x	−y	−y	x	x	y	y
P3	x	x	y	y	−x	−x	−y	−y
P4	−y	off	x	off	y	off	−x	off
P5	y	y	−x	−x	−y	−y	x	x
P6	−y	−y	x	x	y	y	−x	−x
P7	y	y	−x	−x	−y	−y	x	x
P8	x	x	y	y	−x	−x	−y	−y
P9	y	y	−x	−x	−y	−y	x	x
Receiver	y	−y	−x	x	−y	y	x	−x

Note. Additionally, the CYCLOPS scheme was employed, yielding a 32-step phase cycle. The rf pulses Pi ($i = 1$–9) correspond to those of Fig. 1b. The 2θ pulse in the middle of the evolution period was switched on and off between successive phase cycle steps.

LM and DO behave in the same way under the phase cycle of the rf pulses the elimination of ZQ and DQ coherences in LM experiments could also be achieved by choosing the t_1 evolution period longer than the longest value of $T_{2,\mathrm{ZQ}}$, and $T_{2,\mathrm{DQ}}$ relaxation times. The inhomogeneities of the static magnetic field do not affect the life time of the ZQ coherence (*25*). In the experiments for excitation of DO, the orthogonality of the phases of the first θ pulse and the $\theta/2$ pulse (cf. Fig. 2b) allows the excitation of the MQ coherences of odd order for the spin system starting from z polarization (*29, 30*). Therefore, ZQ coherence will not be excited in this case. The single-quantum and MQ coherences of higher order (i.e., $|p| \geq 3$) are filtered out by the combined effect of phase cycle and fast dephasing during the t_1 period. Partial filtration of LM is achieved by the 2θ radio-frequency pulse applied in the middle of the evolution period which is switched on and off between successive phase cycling steps (cf. Table 3).

TABLE 2
Basic Phase Cycling Scheme Used for Recording DQ Filtered Signals

	Radio-frequency pulse and receiver phases			
P1	x	y	−x	−y
P2	−x	−y	x	y
P3	x	y	−x	−y
P4	−y	x	y	−x
P5	y	−x	−y	x
P6	−y	x	y	−x
P7	y	−x	−y	x
P8	x	y	−x	−y
P9	y	−x	−y	x
Receiver	y	−y	y	−y

Note. Additionally, the CYCLOPS scheme was employed, yielding a 16-step phase cycle. The rf pulses Pi ($i = 1$–9) correspond to those in Fig. 1b. In this experiment a 2θ pulse (pulse P4) was applied in the middle of the evolution period.

TABLE 3
Basic Phase Cycling Scheme Used for Recording the DO Multipolar Spin State

	Radio-frequency pulse and receiver phases							
P1	x	x	y	y	−x	−x	−y	−y
P2	−x	−x	−y	−y	x	x	y	y
P3	y	y	−x	−x	−y	−y	x	x
P4	−y	off	x	off	y	off	−x	off
P5	y	y	−x	−x	−y	−y	x	x
P6	−y	−y	x	x	y	y	−x	−x
Receiver	y	y	−x	−x	−y	−y	x	x

Note. Additionally, the CYCLOPS scheme was employed, yielding a 32-step phase cycle. The rf pulses Pi ($i = 1$–6) correspond to those of Fig. 2b.

4. RESULTS AND DISCUSSION

4.1. ^1H Dipolar Encoded Longitudinal Magnetization

The possibility of measuring signals filtered by ^{1}H dipolar encoded LM using the NMR-MOUSE and the pulse sequence presented in Fig. 1b is demonstrated by the LM decay curves recorded on the two natural rubber samples NR1 and NR5. These curves are shown in Fig. 3 for the full relevant range of the excitation/reconversion times. In the initial regime of the excitation/reconversion times the decay is dominated by a τ^2 dependence as revealed by Eq. [10]. This is supported by the expanded dipolar encoded LM decay curves in the inset of Fig. 3. Moreover, the effect of transverse relaxation of the SQ coherences during excitation and reconversion periods is not present, being linear in τ for the initial time regime. The signal-to-noise ratio is relatively good making possible a quantitative evaluation of residual dipolar couplings.

For the same natural rubber samples the ^{1}H dipolar encoded LM decays were recorded on a solid-state Bruker DSX 500 NMR spectrometer using the same pulse sequence (cf. Fig. 1b) with a pulse flip angle of about $\theta = 60^\circ$. The signal decays are shown in Fig. 4 together with the initial τ^2 dependence (inset). With the help of Eq. [10] we obtain the ratio of the square of the ^{1}H residual dipolar couplings for the natural rubber samples NR1 and NR5 as

$$\langle\bar{\omega}_{\mathrm{D}}^2\rangle_{\mathrm{NR5}}^{\mathrm{LM}} / \langle\bar{\omega}_{\mathrm{D}}^2\rangle_{\mathrm{NR1}}^{\mathrm{LM}} \cong 3.3$$

from the data presented in the inset of the Fig. 4, and

$$\langle\bar{\omega}_{\mathrm{D}}^2\rangle_{\mathrm{NR5}}^{\mathrm{LM}} / \langle\bar{\omega}_{\mathrm{D}}^2\rangle_{\mathrm{NR1}}^{\mathrm{LM}} \cong 3.1$$

from the data shown in Fig. 3. Within the limit of the experimental error these ratios are in a good agreement thus showing that the approximations involved in the derivation of Eq. [10] are justified. Moreover, the residual dipolar couplings measured in homogeneous and inhomogeneous magnetic fields differ by

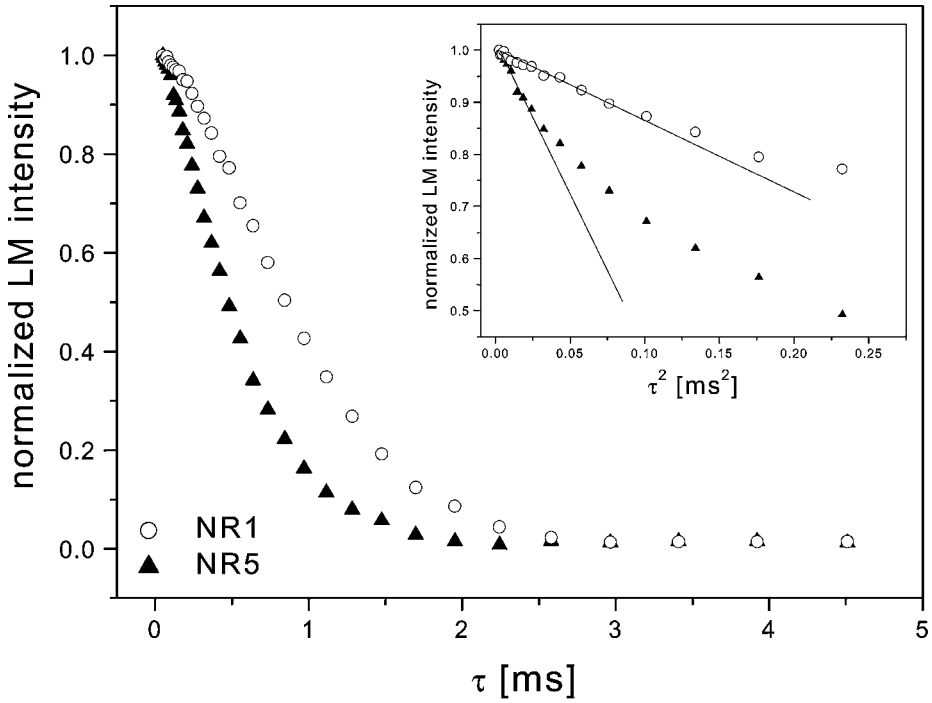

FIG. 3. ^{1}H normalized dipolar encoded LM decay curves for the natural rubber samples NR1 (△) and NR5 (●) which differ in crosslink density. The decay curves have been recorded with the NMR-MOUSE using the pulse sequence of Fig. 1b and the phase cycle of Table 1. The dipolar encoded LM signals were normalized to the intensity of the Hahn echo recorded with the same echo time as that used for the decay curves. The inset shows the linear dependence on τ^2 (solid lines) for the decay curves in the initial excitation/reconversion regime.

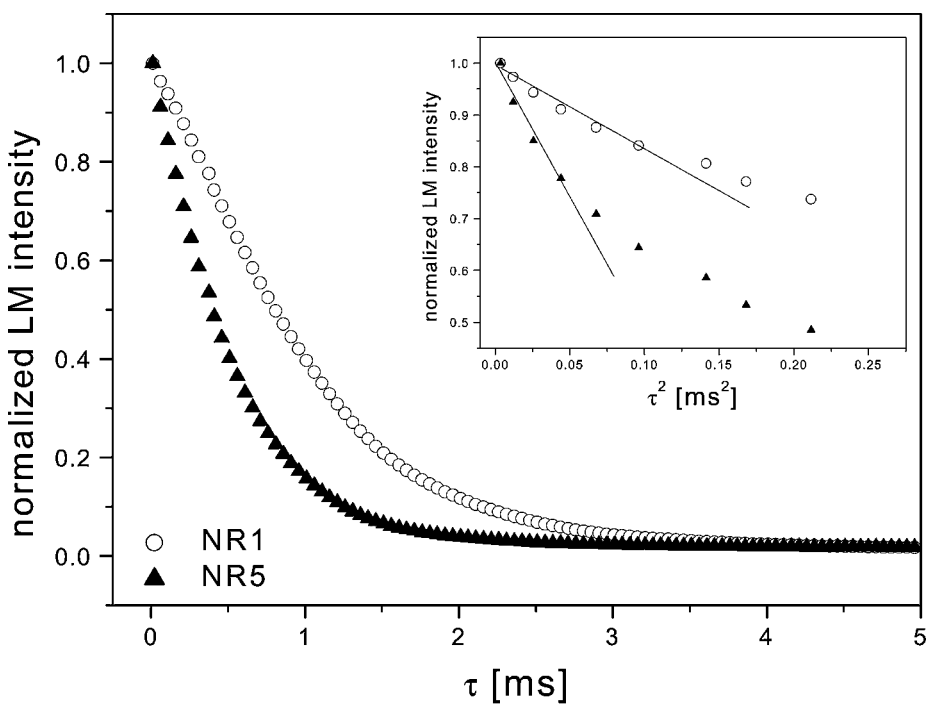

FIG. 4. ^{1}H normalized dipolar encoded LM decay curves for the natural rubber samples NR1 (△) and NR5 (●) with different crosslink densities measured using a solid-state Bruker DSX 500 NMR spectrometer. The decay curves have been recorded using the pulse sequence of Fig. 1b and the phase cycle of Table 1 with a pulse flip angle of about $\theta = 60^\circ$ and the pulse delays identical with those used in the measurements with the NMR-MOUSE. The acquisition was performed without employing a Hahn echo and the LM signals were normalized to the initial intensity of the time-domain signal. The inset shows the linear dependence on τ^2 (solid lines) for the decay curves in the initial excitation/reconversion regime.

about 10% proving that the NMR-MOUSE can provide quantitative values for ratios of the ^{1}H total residual dipolar couplings for elastomers. We can remark here that in the regime of long excitation times, the dipolar encoded LM decays could be slightly different for the measurements performed with the NMR-MOUSE and high-field NMR spectrometers as a result of a possible field dependence of the transverse relaxation rate.

Proton dipolar encoded LM decay curves were also measured using the NMR-MOUSE for the natural rubber band NR1 in the relaxed state (extension ratio $\lambda = 1$) and strained to $\lambda = 2.25$. The extension ratio under an uniaxial force is defined as $\lambda = L/L_0$ where L is the length of the sample under the action of uniaxial force F and L_0 is the length of the sample for $F = 0$. Under mechanical stress the segmental order is increased in elastomers (see Ref. (*31, 32*), and references therein) and therefore, the residual dipolar couplings will increase. This effect is evident in the dipolar encoded LM decay curves presented in Fig. 5. The ratio of the squares of ^{1}H residual dipolar couplings can be obtained from the slopes of the dipolar encoded LM decays shown in the inset of Fig. 5

$$\langle\bar{\omega}_{\mathrm{D}}^2\rangle_{\lambda=2.25}^{\mathrm{LM}} / \langle\bar{\omega}_{\mathrm{D}}^2\rangle_{\lambda=1}^{\mathrm{LM}} \cong 1.43.$$

This value is close to the ratio

$$\langle\bar{\omega}_{\mathrm{D}}^2\rangle_{\lambda=2.25}^{\mathrm{LM}} / \langle\bar{\omega}_{\mathrm{D}}^2\rangle_{\lambda=1}^{\mathrm{LM}} \cong 1.24$$

measured by the same techniques on a different natural rubber band using a Bruker DSX-200 spectrometer (*33*). This is due to the different values of the cross-link density of the investigated elastomers.

4.2. ^{1}H Double-Quantum Build-up and Decay Curves

Proton DQ build-up curves have been recorded with the NMR-MOUSE sensor for a relaxed (i.e., $\lambda = 1$) and stretched ($\lambda = 2.25$) natural rubber NR1 sample. The data are shown in Fig. 6. The low signal-to-noise ratio in the initial regime of the build-up curves leads to errors in the estimation of the residual dipolar couplings. Nevertheless, the DQ build-up curves clearly show a dependence on the λ ratio. The maxim of the DQ build-up curves (dashed lines in Fig. 6) is shifted to an earlier time for the stretched elastomer. This fact is mainly a combination of two effects: (i) the differences in the ^{1}H residual dipolar couplings i.e.,

$$\langle\bar{\omega}_{\mathrm{D}}^2\rangle_{\lambda=2.25}^{\mathrm{DQ}} > \langle\bar{\omega}_{\mathrm{D}}^2\rangle_{\lambda=1}^{\mathrm{DQ}},$$

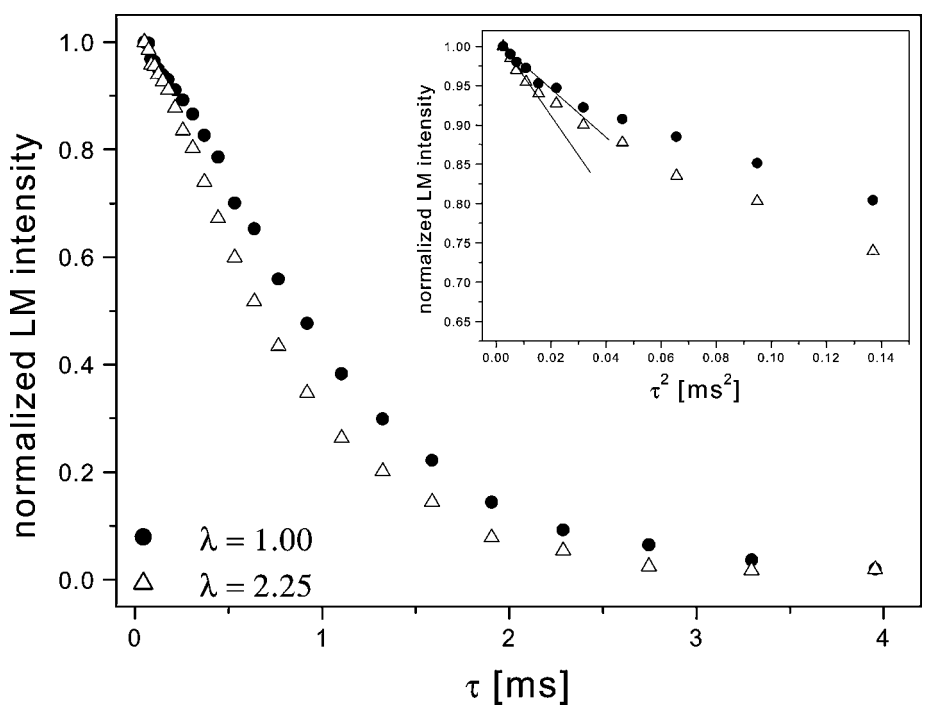

FIG. 5. ^{1}H normalized dipolar encoded LM decay curves for the natural rubber sample NR1 for two elongation ratios $\lambda = 1.00$ (●) and $\lambda = 2.25$ (△) measured by the NMR-MOUSE. The decay curves were recorded using the same procedure and parameters as discussed in Fig. 3. The inset shows the linear dependence on τ^2 (solid lines) for the decay curves in the initial excitation/reconversion regime.

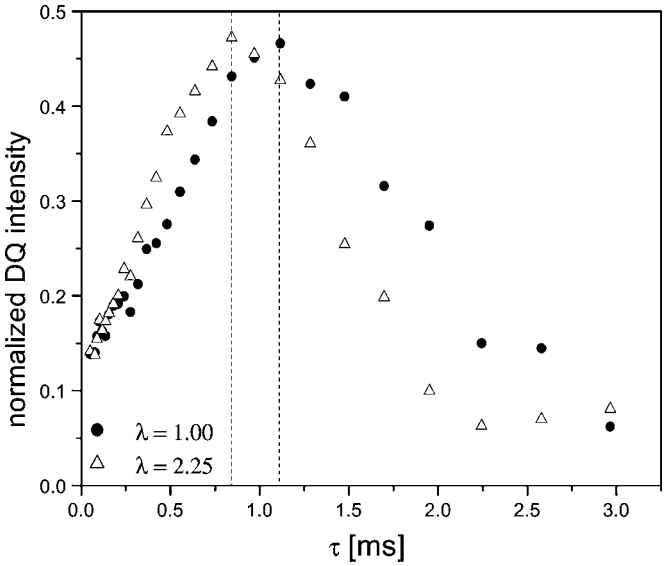

FIG. 6. ^{1}H normalized DQ built-up curves for the natural rubber sample NR1 for two elongation ratios $\lambda = 1.00$ (●) and $\lambda = 2.25$ (△) measured by the NMR-MOUSE. The build-up curves have been recorded using the pulse sequence of Fig. 1b and the phase cycle of Table 2. The DQ signals were normalized to the intensity of the Hahn echo recorded with the same echo time as that used for build-up curves. The position of the maxim for each build-up curve is marked by a dashed line.

and (ii) differences in the transverse relaxation rates of the single-quantum coherences (i.e., $T_2(\lambda = 2.25) < T_2(\lambda = 1)$). The latter effect is shown in Fig. 7 where the Hahn echo decays were recorded with the NMR-MOUSE for the two elongation ratios discussed above. The long decay components were fitted with an exponential function and different effective transverse relaxation times $T_2(\lambda = 1) = 1.79$ ms and $T_2(\lambda = 2.25) = 1.12$ ms are obtained.

A better signal-to-noise ratio can be obtained using filtered DQ decay curves recorded with the MERE method (*12*). The data measured in the initial regime of the excitation and reconversion periods are presented in Fig. 8. From the linear τ^2 dependence it is possible to evaluate the ratio of the square of the residual dipolar couplings (*12*). We obtain the value

$$\langle\bar{\omega}_{\mathrm{D}}^2\rangle_{\lambda=2.25}^{\mathrm{DQ}} / \langle\bar{\omega}_{\mathrm{D}}^2\rangle_{\lambda=1}^{\mathrm{DQ}} \cong 1.35$$

which is in a good agreement with the value of 1.43 measured from dipolar encoded LM decays (see above).

It is well known that the residual dipolar and quadrupolar couplings depend on the angle between the direction of the static magnetic field B_0 and the direction of the uniaxial applied force for elastomer materials (*31, 32*). In the case of NMR-MOUSE, because of the B_0 inhomogeneities an effective orientation angle (Θ) can be defined between the direction of the applied force and the axis oriented perpendicular on the permanent magnet faces. The angular dependence of the ^{1}H DQ filtered signals measured with the NMR-MOUSE for NR1 band with $\lambda = 2.5$ and excitation/reconversion times of $\tau = 0.5$ ms and $\tau = 1.6$ ms are shown in Fig. 9. These times correspond to the rising part and the decaying part of the DQ build-up curve. The angular dependences show a broad

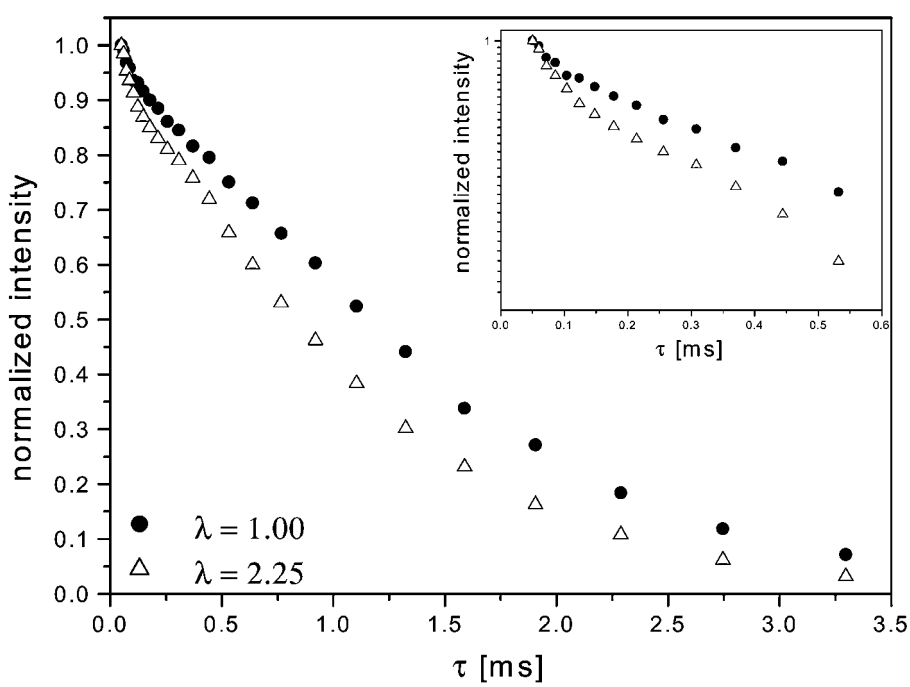

FIG. 7. ^{1}H normalized Hahn echo decay curves of the natural rubber samples NR1 for two elongation ratios $\lambda = 1.00$ (●) and $\lambda = 2.25$ (△) measured by NMR-MOUSE. The inset shows the Hahn echo decays in the initial time regime.

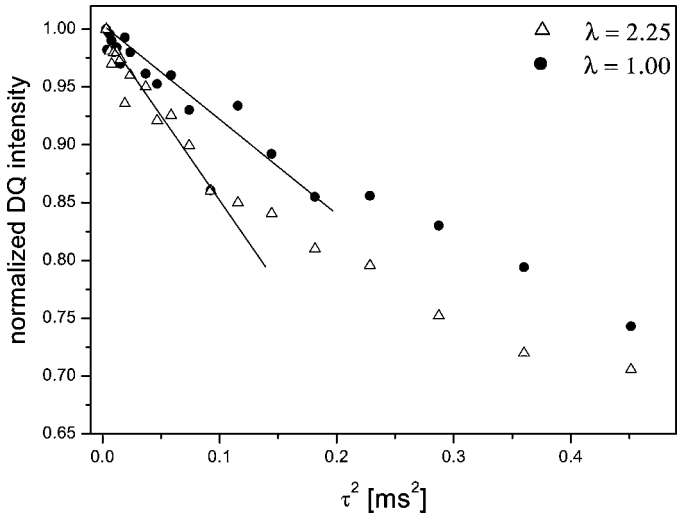

FIG. 8. ^{1}H normalized DQ decay curves of the natural rubber sample NR1 for two elongation ratios $\lambda = 1.00$ (●) and $\lambda = 2.25$ (△) measured by the NMR-MOUSE in the initial excitation/reconversion time regime. The decay curves have been recorded using the MERE pulse sequence (*12*). The DQ signals were normalized to the intensity of the Hahn echo recorded with the same echo time as that used for the decay curves. The solid lines shows the linear dependence on τ^2 for the decay curves in the initial excitation/reconversion regime.

minimum and a broad maximum around an angle close to the magic angle of $\Theta_m = 54.7^\circ$. The rising part of the DQ build up curve is dominated by the residual dipolar couplings and is described by a function which contain terms of the form

$$\langle\langle(\bar{\omega}_{\rm D})^{2n}\rangle\rangle_V \propto \langle(P_2(\cos\Theta(\vec{r})))^{2n}\rangle_V, \quad (n = 1, 2, 3\ldots),$$

where $P_2(\cos\Theta(\vec{r}))$ is the Legendre polynomial of second order in $\cos\Theta(\vec{r})$. The angle $\Theta(\vec{r})$ is the angle between the local static magnetic field $\vec{B}_0(\vec{r})$ and the force $\vec{F}$. The average over the sensitive volume of the NMR-MOUSE is denoted by $\langle(\ldots)\rangle_V$ and is taking into account the distribution in the orientation of $\vec{B}_0$. It is obvious that the intensity of the DQ filtered signal has a minimum value at the magic angle Θ_m when, in some region of the sensitive volume, $\vec{B}_0$ is oriented at this angle relative to $\vec{F}$. Furthermore, the strong inhomogeneities in the orientation of the static magnetic field make the ratios $S_{\rm DQ}(\Theta = 0)/S_{\rm DQ}(\Theta_m)$ and $S_{\rm DQ}(\Theta = 0)/S_{\rm DQ}(\Theta = 90^\circ)$ different from the expected Θ dependence given by the Legendre polynomial of second order (cf. Fig. 9). In the decay region of the DQ build-up curve the intensity of the filtered signal is dominated by the transverse relaxation (T_2) of the SQ coherences. It was shown that $1/T_2$ has a strong anisotropy in oriented tissues (*34*, and references therein) having a minimum for the magic angle. Therefore, the attenuation of the DQ filtered signal is minimum and the signal has a maximum value as it is evident from the Fig. 9. In this regime of the excitation/reconversion the anisotropy of the DQ filtered signal is reduced compared to the initial regime because of the opposite contribution to the signal intensity given by the residual dipolar couplings and transverse relaxation. A detail analysis of this anisotropy is currently under investigation and will be published elsewhere.

4.3. ^{1}H Dipolar Order Build-up Curves

Build-up curves of proton dipolar order originating from the residual dipolar couplings can be measured in elastomers using the NMR-MOUSE, i.e., in the presence of strongly inhomogeneous magnetic fields. Figure 10 shows two DO build-up curves recorded with the pulse sequence of Fig. 2b for the NR1 and NR5 samples by the NMR-MOUSE sensor (cf. Fig. 10a) and the Bruker DSX 500 spectrometer (cf. Fig. 10b). As expected, the rising initial slope of the DO build-up curve for the natural rubber NR5 with the higher value of the crosslink density is larger than that of the sample NR1. The position of the maxima of the curves (dashed lines) are shifted as expected from the differences in residual dipolar couplings and transverse relaxation rates. Nevertheless, the maxima of the DO build-up curves measured with Bruker DSX 500 spectrometer are both shifted to lower values compared to those measured with NMR-MOUSE. This effect is related to the differences between the transverse relaxation rates of single-quantum coherences at 500 MHz and 20 MHz.

From Figs. 10a and 10b it is evident that the efficiency of detecting signals filtered according to DO in inhomogeneous low magnetic fields is almost an order of magnitude lower compared to that of experiments performed in homogeneous fields. Therefore, no effort was done to extract the ratio of the

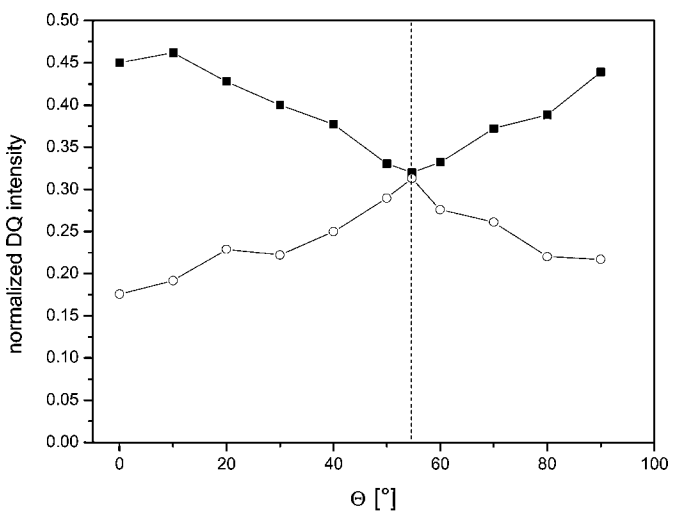

FIG. 9. Angular dependence of the ^{1}H normalized DQ build-up curves for the natural rubber sample NR1 with elongation ratio $\lambda = 2.5$ measured by the NMR-MOUSE. The angle between the direction of the uniaxial stress force and the axis perpendicular to the faces of the permanent magnet is denoted by Θ. The DQ filtered signals have been recorded using the pulse sequence of Fig. 1b and the phase cycle of Table 2 for $\tau = 0.5$ ms (■) and $\tau = 1.6$ ms (○). The DQ signals were normalized to the intensity of the Hahn echo recorded with the same echo time as that used for DQ filtered signals.

^{1}H residual dipolar couplings from the experiments performed with NMR-MOUSE.

The DO build-up curves are also sensitive to the strain of elastomers. This effect is shown for the sample NR1 for the two elongation ratios $\lambda = 1$ and $\lambda = 2.25$ (cf. Fig. 11). The maxima of both DO build-up curves are shifted to the shorter times compared to the corresponding DQ build-up curves (cf. Fig. 6). This effect is due to the differences in the encoding efficiency of ^{1}H residual dipolar couplings. This efficiency of dipolar encoding is higher for the DO build-up curves compared to that for the DQ build-up curves as can be seen from the different multiplication factors of the $\langle(\bar{\omega}_D)^2\rangle\tau^2$ terms in Eqs. [14] and [11], respectively.

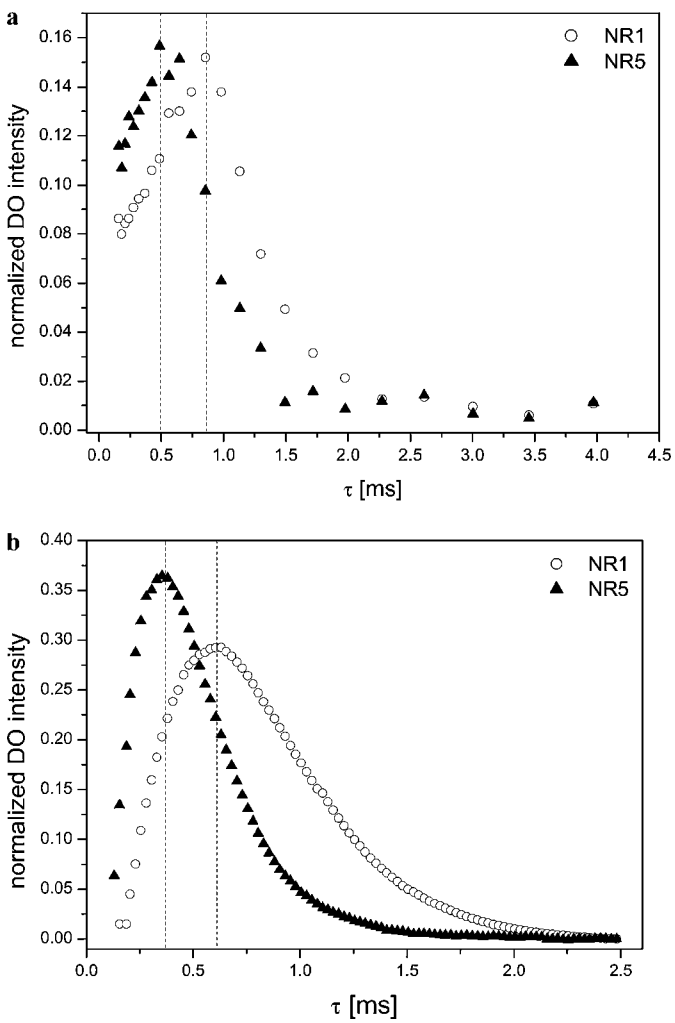

FIG. 10. ^{1}H normalized DO build-up curves for the natural rubber samples NR1 (○) and NR5 (▲) with different crosslink densities measured by the (a) NMR-MOUSE and (b) the Bruker DSX 500 NMR spectrometer. The build-up curves have been recorded using the pulse sequence of Fig. 2b and the phase cycle of Table 3. The DO signals were normalized to the intensity of the Hahn echo recorded with the same echo time as that used for the DQ build-up curves. The positions of the maxima for each build-up curve are marked by dashed lines.

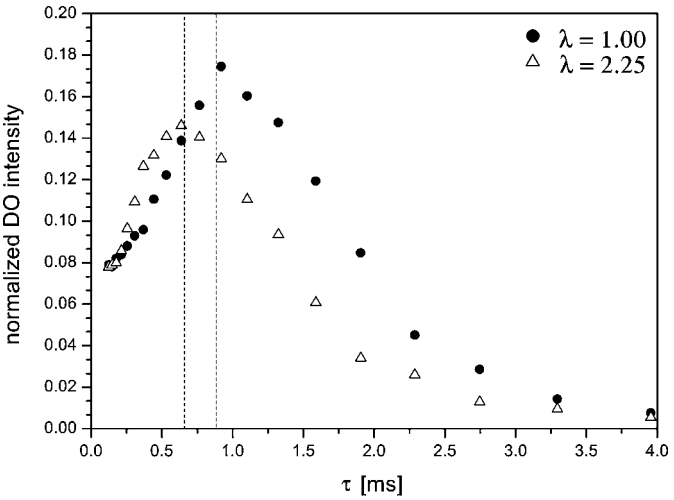

FIG. 11. ^{1}H normalized DO build-up curves for the natural rubber sample NR1 for two elongation ratios $\lambda = 1.00$ (●) and $\lambda = 2.25$ (△) measured by the NMR-MOUSE. The build-up curves have been recorded using the pulse sequence of Fig. 2b and the phase cycle of Table 3. The DO signals were normalized to the intensity of the Hahn echo recorded with the same echo time as that used for build-up curves. The positions of the maxima for each build-up curve are marked by dashed lines.

5. CONCLUSIONS

The possibility of exciting and detecting various multipolar spin states like dipolar encoded longitudinal magnetization, double-quantum coherences, and dipolar order in strongly inhomogeneous magnetic fields was proved by experiments with the NMR-MOUSE. To partially mimic the effects of the field inhomogeneities on the excitation/reconversion evolution of various multipolar spin states the methods employed were tested on a solid-state Bruker DSX 500 NMR spectrometer using the same pulse sequences as for the NMR-MOUSE with an arbitrary value of the pulse flip angle. As was shown by the evaluation of the spin system response for an ensemble of dipolar coupled spin-1/2 pairs the distribution of pulse flip angles in the inhomogeneous magnetic fields leads to the simultaneous excitation of many spin states. The success of filtering individual multipolar spin states in inhomogeneous fields is related mainly to the fact that even in inhomogeneous fields the phases of the radio-frequency pulses are the same for all the voxels in the sample.

This mobile NMR sensor can excite and detect DQ coherences for more rigid solids compared to the elastomers. The limitations are related to the death time, pulse length, and signal-to-noise ration which are currently available with this device working at low magnetic field.

Compared to MQ coherences, the LM spin state is characterized by a larger NMR signal which is an important feature especially for low-frequency NMR sensors like the NMR-MOUSE. In principle, the LM spin state is excited simultaneously for spins in isotropic and anisotropic/restricted environments.

Nevertheless, the decay of dipolar encoded LM with increasing the excitation/reconversion times is related to the solid-like behavior of heterogeneous soft solids.

The possibility to detect signals filtered according to ^{1}H dipolar order which originate only from the spins in the solid-like environments expands the sphere of applications of the NMR-MOUSE for measuring macroscopic properties of elastomers and other soft solid matter affected by the segmental dynamics. The Jeener–Broekaert scheme (*21*) is not the only method which can be employed to produce DO but also adiabatic demagnetization in the rotating frame can be successfully used with the NMR-MOUSE. The efficiency of this technique is expected to be higher than that of the Jeener–Broekaert method.

The sensitivity of the dipolar encoded LM, DQ coherences and DO to differences in cross-link density and strain was shown for samples of natural rubber. This extends the panoply of NMR parameters that can be used with the NMR-MOUSE for investigation of elastomer materials. Moreover, the DQ filtered signals was shown to be sensitive to the angle between the direction of the applied uniaxial force and the direction of the axis along the permanent magnet poles. The possibility of recording proton dipolar encoded LM and DQ filtered NMR signals suggests the use of the NMR-MOUSE for characterization of tissue order in connective tissues, muscles, and blood vessels (*34*). These techniques can be also applied to the investigation of ^{23}Na nuclei in biological tissues.

ACKNOWLEDGMENTS

This work was supported by grants from the Deutsche Forschungsgemeinschaft (DE 780/1-1) and by the Bundesministerium für Bildung und Forschung (BMBF) under the German–Israeli Project Cooperation (DIP). The authors are also grateful to K. Unseld and V. Hermann, Dunlop GmbH, Hanau, for providing the samples and helpful information. The authors acknowledge stimulating discussions with Gil Navon and Uzi Eliav.

REFERENCES

1. G. Eidmann, R. Savelsberg, P. Blümler, and B. Blümich, The NMR-MOUSE, a mobile universal surface explorer, *J. Magn. Reson. A* **122,** 104–109 (1996).
2. G. Guthausen, A. Guthausen, F. Balibanu, R. Eymael, K. Hailu, U. Schmitz, and B. Blümich, Soft-matter analysis by the NMR-MOUSE, *Macromol. Mater. Eng.* **276/277,** 25–37 (2000).
3. A. Guthausen, G. Zimmer, P. Blümler, and B. Blümich, Analysis of polymer materials by surface NMR via the MOUSE, *J. Magn. Reson*. **130,** 1–7 (1998).
4. B. Blümich, "NMR Imaging of Materials," Clarendon Press, Oxford (2000).
5. R. L. Kleinberg, "Encyclopedia of Nuclear Magnetic Resonance," Vol. 8, Chap. "Well logging," pp. 4960–4969, Wiley, Chichester (1996).
6. P. J. McDonald, Stray field magnetic resonance imaging, *Prog. Nucl. Magn. Reson. Spect.* **30,** 69–99 (1997).
7. F. Balibanu, K. Hailu, R. Eymael, D. E. Demco, and B. Blümich, Nuclear magnetic resonance in inhomogeneous magnetic fields, *J. Magn. Reson.* **145,** 246–258 (2000).
8. M. D. Hürlimann and D. E. Griffin, Spin dynamics of Carr–Purcell–Meiboom–Gill-like sequences in grossly inhomogeneous B_0 and B_1 fields and application to NMR well logging, *J. Magn. Reson.* **143,** 120–135 (2000).
9. A. Wiesmath, H. Kühn, R. Fechete, D. E. Demco, and B. Blümich, Integrated dispersion of spin–lattice relaxation time in the rotating frame in strongly inhomogeneous magnetic fields, submitted for publication.
10. M. D. Hürlimann, Diffusion and relaxation effects in general stray field NMR experiments, *J. Magn. Reson*. **148,** 367–378 (2001).
11. A. Wiesmath, C. Gehlen, D. E. Demco, and B. Blümich, unpublished results.
12. A. Wiesmath, C. Filip, D. E. Demco, and B. Blümich, Double-quantum filtered NMR signals in inhomogeneous magnetic fields, *J. Magn. Reson.* **149,** 258–263 (2001).
13. M. Schneider, L. Gasper, D. E. Demco, and B. Blümich, Residual dipolar couplings by ^{1}H dipolar encoded longitudinal magnetization, double- and triple-quantum nuclear magnetic resonance in cross-linked elastomers, *J. Chem. Phys.* **111,** 402–415 (1999).
14. M. Schneider, D. E. Demco, and B. Blümich, ^{1}H NMR imaging of residual dipolar couplings in cross-linked elastomers: Dipolar-encoded longitudinal magnetization, double-quantum, and triple-quantum filters, *J. Magn. Reson.* **140,** 432–441 (1999).
15. U. Eliav and G. Navon, A study of dipolar interactions and dynamic processes of water molecules in tendon by ^{1}H and ^{2}H homonuclear and heteronuclear multiple-quantum-filtered NMR spectroscopy, *J. Magn. Reson.* **137,** 295–310 (1999).
16. G. J. Bowden and W. D. Hutchison, Tensor operator formalism for multiple-quantum NMR. 1. Spin-1 nuclei, *J. Magn. Reson.* **67,** 403–414 (1986).
17. G. J. Bowden, W. D. Hutchison, and J. Khachan, Tensor operator formalism for multiple-quantum NMR. 2. Spin 3/2, 2, and 3/2 and general I, *J. Magn. Reson.* **67,** 415–437 (1986).
18. T. Karlsson, A. Brinkmann, P. J. E. Verdegem, J. Lugtenburg, and M. H. Levitt, Multiple-quantum relaxation in the magic-angle-spinning NMR of ^{13}C spin pairs, *Solid State Nucl. Magn. Reson.* **14,** 43–58 (1999).
19. G. Jaccard, S. Wimperis, and G. Bodenhausen, Multiple-quantum NMR spectroscopy of $S = 3/2$ spins in isotropic phase: A new probe for multiexponential relaxation, *J. Chem. Phys.* **85,** 6282–6293 (1986).
20. U. Eliav, H. Shinar, and G. Navon, The formation of a second-rank tensor in ^{23}Na double-quantum filtered NMR as an indicator for order in a biological tissue, *J. Magn. Reson.* **98,** 223–231 (1992).
21. J. Jeener and P. Broekaert, Nuclear magnetic resonance in solids: Thermodynamic effects of a pair of radio-frequency pulses, *Phys. Rev.* **157,** 232–245 (1967).
22. R. Kemp-Harper and S. Wimperis, Detection of the interaction of sodium ions with ordered structures in biological systems. Use of the Jeener–Broekaert expriment, *J. Magn. Reson. B* **102,** 326–331 (1993).
23. S. P. Brown and S. Wimperis, Extraction of homogeneous ^{23}Na NMR linewidth from two-dimensional Jeener–Broekaert spectra, *J. Magn. Reson. B* **109,** 291–300 (1995).
24. R. Kemp-Harper, B. Wickstead, and S. Wimperis, Sodium ions in ordered environments in biological systems: Analysis of ^{23}Na NMR spectra, *J. Magn. Reson.* **140,** 351–362 (1999).
25. R. R. Ernst, G. Bodenhausen, and A. Wokaun, "Principles of Nuclear Magnetic Resonance in One and Two Dimensions," Clarendon, Oxford (1987).
26. M. Munowitz and A. Pines, Principles and applications of multiple-quantum NMR, *Adv. Chem. Phys.* **66,** 1–152 (1987).

27. R. Kimmich, "NMR, Tomography, Diffusometry, Relaxometry," Springer-Verlag, Berlin/New York (1997).

28. J. P. Cohen Addad, NMR and fractal properties of polymeric liquids and gels, *Prog. Nucl. Magn. Reson. Spec.* **25,** 1 (1993).

29. Y. Ba and W. S. Veeman, Experimental detection of multiple-quantum coherence transfer in coupled spin solids by multi-dimensional NMR experiments, *Solid State Nucl. Magn. Reson.* **2,** 131–141 (1993).

30. R. Tycko, Selection rules for multiple-quantum NMR excitation in solids: Derivation from time-reversal symmetry and comparison with simulations and ^{13}C NMR experiments, *J. Magn. Reson.* **139,** 302–307 (1999).

31. P. T. Callaghan and E. T. Samulski, Molecular ordering and the direct measurement of weak proton–proton dipolar interactions in rubber network, *Macromolecules* **30,** 113–122 (1997).

32. P. Sotta and B. Deloche, Uniaxiality induced in a strained poly(dimethylsiloxane) network, *Macromolecules* **23,** 1999–2007 (1990).

33. M. Schneider, D. E. Demco, and B. Blümich, NMR images of proton residual dipolar coupling from strained elastomers, *Macromolecules* **34,** 4013–4026 (2001).

34. R. Haken and B. Blümich, Anisotropy in tendon investigated *in vivo* by a portable NMR scanner the NMR-MOUSE, *J. Magn. Reson.* **144,** 195–199 (2000).